CHAPTER-8

ATYPICAL NONLINEAR WAVES IN A SELF-GRAVITATING COLLISIONAL DUSTY PLASMA WITH ACTIVE ION-INERTIA

Abstract: *We present an atypical theoretical model to study gravito-electrostatic mode-fluctuations in self-gravitating inhomogeneous interstellar dust molecular cloud (DMC) on the astrophysical fluid scales of space and time. The main focus is centered around investigating the influence of self-consistent dynamic ion-inertial effects on the stability behavior. Methodological application of standard multiple scaling techniques reduces the basic plasma structure equations into a unique pair of the decoupled Korteweg-de Vries (KdV) system governing the weakly nonlinear fluctuations. In contrast, the fully nonlinear counterparts are shown to evolve as a new gravito-electrostatically coupled pair of the Sagdeev energy-integral equations. Numerical shape-analysis shows the excitation of two distinct eigenmode classes, electrostatic compressive solitons and self-gravitational rarefactive solitons, with singular parametric features portrayed in detail. The graphical setup reflects some new plasma conditions in realistic interstellar parameter window previously remaining unexplored. It is seen that the inertial ions play a destabilizing influential role leading to enhanced fluctuations towards establishing a new reorganized gravito-electrostatic equilibrium setup. A substantially good qualitative correspondence, but with minor quantitative modifications due to the considered ion-inertial correction, is found to exist in comparison with those by the earlier inertialess ion-theories and multispace satellite-based observations. The main implications relevant to space and astrophysical contexts are summarily highlighted together with concise future directions emphasized.*

8.1 INTRODUCTION

Plasmas and the dust are two main ingredients of the universe. The interplay between both has opened up a new and fascinating research domain of astrophysical plasmas. The study of such astrophysical dusty plasma consisting of the micron-sized dust grains has attained more interest because of its vital role in understanding different collective processes such as mode modifications,

evolutions, excitations of new nonlinear eigenmodes, and coherent structures like solitons, shock, vortices, etc. [1-4]. A soliton is a self-reinforcing solitary wave (a wave packet pulse) that maintains its shape while it progress at a constant velocity. Similarly, shock wave is defined as a type of propagating disturbance when a wave moves faster than the speed of sound in a liquid, gas, or plasma. The dust grains are immersed in ambient plasmas and radiative environments, and become electrically charged by various processes; the most simple one being capture of the electrons and ions from the background plasma. The other charging mechanism of the dust grains in space are secondary electron emission, photoelectric effect, and so forth [1-2]. So, the fluctuating dust-charge behaves as a new dynamical variable. The dust response time scale is small ($\tau_{dr} \sim 10^{-3}$ s), whereas the dust-charging time is very small ($\tau_{ch} \sim 10^{-8}$ s) in normal plasma conditions [5-6]. Thus, the effect of the dust motion is too slow to neutralize the electron-ion currents [5-7]. In such situations, the grain-charge may justifiably be considered to be static, at least in principle, in the characteristic time-scale of low-frequency waves like in the present investigation.

It is well established that the charged grains have significant impact in the mechanisms involving excitation, evolution, and propagation of low frequency nonlinear eigenmodes in the interplanetary space, interstellar medium, circumstellar space, interstellar dust molecular clouds (DMCs), comets, planetary rings, Earth's environments, and so on [1-2, 8-9]. The existence of such modified eigenmodes spanning from laboratory-to-galactic scales have widely been studied theoretically [1, 5, 10-11] as well as experimentally [12-13]. The existence of massive partially ionized dust grains in the DMCs indeed develops significant self-gravitational effects on the Jeans scale. Moreover, the coupling of the self-gravitational attraction (Newtonian) developed by the grain-mass and the electrostatic repulsion (Coulombic) sourced by the grain-charge with partial ionization leads to the pulsational mode instability [14-15]. The gravito-electrostatic interplay, after being stabilized by counter-force-balancing, leads to the formation of bounded large-scale structures (~Jeans-scale) attributed to self-gravitational condensation. Thus, different sorts of nonlinear eigenmodes resulting out of such instabilities play a substantial role in understanding the basic physics of formation-evolution processes of stars and other galactic structures [1-3]. The presence of the dust with wide-range mass spectrum and subsequent excitation of different nonlinear eigenmodes in space and astrophysical environments have also been confirmed by remote satellite-based (like Viking, Freja, Polar, FAST, etc.) observations [16-19]. Notwithstanding, it may be noted that theoretical formalisms for meticulously interpreting such

observations on the nonlinear wave signatures are yet to be well formulated. To be more specific, nonlinear gravito-electrostatic disturbances in self-gravitating collisional plasmas with the effective ion-inertia taken into account are yet to be explored.

The plasmas in space and astrophysical environments are well-known to consist of numerous massive ionic components contributing to various wave-instability phenomena [20]. The ion-inertia, although weak but finite in comparison with the massive grains ($m_i/m_d \sim 10^{-15} - 10^{-8}$), might have some dominant interesting influences on the excitation processes and associated evolutionary dynamics of the normal modes in wide-spatially extended systems [9, 20-23]. Thus, it is questionable to treat the heavy ions as the Boltzmanian particles in the analyses as usual tradition. Keeping this top importance in mind, many authors have carried out linear stability analyses of collisionless (and collisional) dusty plasmas with the ion-inertial effects via non-static ion response included [9, 21-22]. The ionic gravity plays in quantitative enhancement of the self-gravitational cloud collapse only, an outcome of greater time-scale needed to incorporate the ion dynamic response in the electrostatic field-field coupling of the positive ions and negatively charged grains. In contrast, in case of positively charged grains, the gravitating ions develop strong electrostatic field fluctuations, which result in slowing down the collapse. In nonlinear regimes, weakly and strongly nonlinear analyses of two [24] and three [20] component dusty plasmas with the ion-inertia considered have also been reported in past. In presence of the non-isothermal electrons and inertial ions with the charge-fluctuating immobile grains, dust ion-acoustic soliton-shock transitions have also been recently reported [25]. But, to the best of our knowledge, nowhere, collisional, strong nonlinearities and self-gravitational effects with the dynamic ion-inertial response are jointly accounted for on the Jeans scales of space and time.

The work in this chapter is thus motivated by the developing curiosity for understanding the evolutionary dynamics of weakly and strongly nonlinear eigenmode structures excitable in a planar one-dimensional (1-D) self-gravitating DMC including all the significant agencies in a hydrodynamic inhomogeneous equilibrium configuration. Both the ionic and dust fluids are assumed to be polytropic in nature with polytropic indices, $\Gamma_i = \Gamma_d = 1$, which correspond to isothermal states. The key stimulus is on the inclusion of the effective ion-inertia and various collisional effects in the evolution of low-frequency gravito-electrostatic eigenmodes by multiscale analysis [26] and the Sagdeev pseudo-potential approaches [27] jointly. It is found that the weakly and strongly nonlinear fluctuations dynamically evolve like a decoupled pair of

Korteweg-de Vries (KdV) and a coupled pair of energy-integral equations, respectively. A detailed numerical analysis as initial value problems by the fourth-order Runge-Kutta method (RK-IV, stationary) and the Finite-Difference method (FD, spatiotemporal) under some judicious plasma multi-parameter variation, previously remaining unexplored, is carried out. The fluctuation structures appear mainly in the form of compressive and rarefactive solitary spectral patterns. We briefly discuss their main applicability in diverse areas like cloud physics, space science and modern astrophysics in understanding self-gravitational collapse, formation and evolution of interstellar structure, star formation, and galactic evolution, etc.

8.2 PHYSICAL MODEL

We consider a simplified multifluid model of unmagnetized, collisional, self-gravitating, inhomogeneous DMC in global quasi-neutral hydrodynamic equilibrium configuration with the dynamic ion-inertial response taken into account on the astrophysical fluid scales of space and time. It consists of the warm gas-phase electrons, the gravitating positive ions and the negatively charged massive dust grains of identical characteristics as shown in figure 8.1. The inertialess electrons are assumed to acquit as the thermal species, described by the Boltzmann distribution law. The cold gravitating ions and the dust grain microspheres behave as isothermal inertial fluids (polytropic indices, $\Gamma_i = \Gamma_d = 1$). All the effects dependent on the ion-inertia are retained in the ion dynamics to see its self-consistent influence on the grainy cloud fluctuations. The dust grains are negatively charged because of the unequal electron-ion fluxes to the grain surface due to higher electron thermal speed [1-3, 15]. For simplicity, we consider static dust-charge under the approximation that the dust charging time-scale is much smaller than the characteristic time scale of low-frequency wave kinetics under study [21].

The self-gravitating plasmas are indeed inhomogeneous in nature [2, 8-9]. However, for simplification, our model is methodologically developed based on the Jeans assumption of self-gravitating uniform homogeneous plasma [28-29]. Thus, the zero-order self-gravitational field is neglected, and the equilibrium is treated initially as 'homogeneous' on the zeroth-order, thereby validating nonlinear local analysis. The efficacious inertial mass of the cloud is collectively contributed by the cold gravitating grains and cold gravitating ions such that $v_{te} >> \omega/k >> v_{ti}, v_{td}$, where v_{te} is the electron thermal speed; ω/k is the phase velocity of the linear fluctuations, the nonlinear counterparts of which are now studied; and v_{ti}, v_{td} are the thermal speeds of the ions and

grains, respectively [9, 20-22]. The adopted simplification ignores the effect of magnetic field on the constituents, differential rotation, viscosity, circulation, dust-charge dynamics, dust-size distribution, etc. The neutral fluid dynamics coupling the background plasma via self-gravitational field is also neglected.

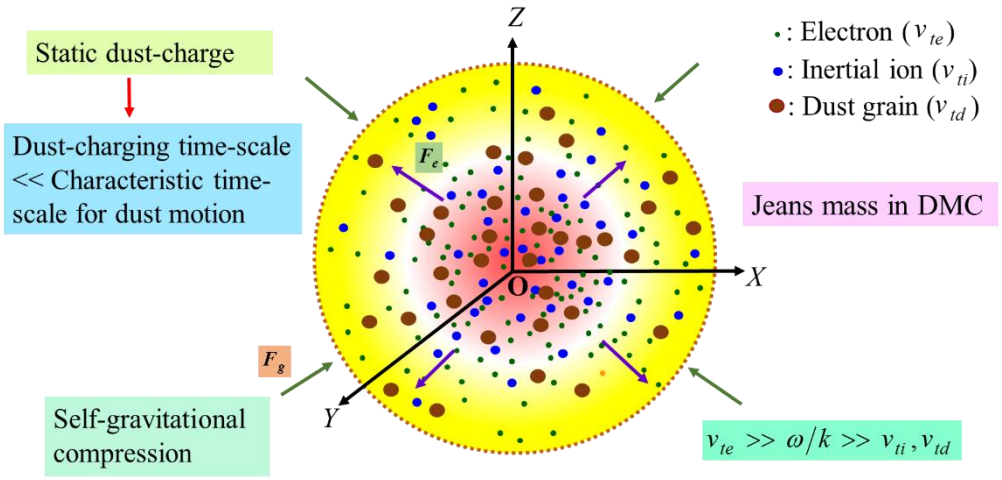

Figure 8.1 *Cartoon showing our considered DMC model.*

It may be pertinent to add that an assumed wide-range spectrum in the grain-mass ($m_d \sim 10^{-21}$-$10^{-9}\ kg$) physically allows a suitable parameter regime, where, the monopolar self-gravitational and bipolar electrostatic forces may become approximately comparable. Thus, if the grain charge-to-mass ratio is such that $Gm_d^2/q_d^2 \sim 0(1)$, the joint interplayed action of the two opposing forces in establishing gravito-electrostatic equilibrium may play an important role in facilitating the formation processes of large-scale equilibrium structures of bounded astrophysical objects via self-gravitational condensation.

8.3 MATHEMATICAL ANALYSES

The considered self-gravitating one-dimensional (1-D) dusty plasma consists of the inertialess Boltzmann electrons, gravitating inertial ions and gravitating inertial dust grains with full ionization. The macroscopic state of such an astrophysical situation can be described by a closed conservative set of the Boltzmann distribution, normal continuity, collisional momentum, and coupling electro-gravitational Poisson equations with all the conventional notations on the required astrophysical scales of space and time [11, 14-15, 21].

8.3.1 Governing Equations

We assume that the phase speed of the fluctuations is much smaller than the electron thermal speed, so the electron volumetric population density in normalized form is represented by the Boltzmann distribution law set out as follows,

$$N_e = \exp(\Phi). \tag{8.1}$$

For the ion and grain inertial fluids, a polytropic law of the form, $p_s = k_s n_s^{\Gamma_s}$, is adopted for the fluid pressure, where Γ_s (with $s = i$ for the ions, and $s = d$ for the dust grains) is the polytropic index of the s^{th} species [1, 30-31] and k_s is a constant of proportionality. In normalized form, the law becomes $P_s = N_s^{\Gamma_s}$. Here, the pressure is normalized by the corresponding equilibrium thermal pressure ($p_{so} = n_{so} T_s$) and density, by the equilibrium density (n_{so}). So, the dynamics of the ionic and dust fluids in normalized form are given by,

$$\frac{\partial N_s}{\partial \tau} + \frac{\partial}{\partial \xi}(N_s M_s) = 0 \text{ , and} \tag{8.2}$$

$$\frac{\partial M_s}{\partial \tau} + M_s \frac{\partial M_s}{\partial \xi} = -\chi_s \frac{\partial \Phi}{\partial \xi} - \Omega_s \left(\frac{T_s}{T_e}\right) \frac{1}{N_s} \frac{\partial P_s}{\partial \xi} - \frac{\partial \Psi}{\partial \xi} - f_s . \tag{8.3}$$

Here, for $s = i$, one has $\chi_i = \Omega_i = \alpha$, and $f_i = F_{id}(M_i - M_d)$. Similarly, for $s = d$, we have $\chi_d = (q_d / e)$, $\Omega_d = 1$, and $f_d = F_{di}(M_d - M_i)$. The term $\alpha \left(= m_d / m_i\right)$ is the grain-to-ion mass ratio; and T_e, T_i , T_d are the temperatures (in eV) of the electrons ($q_e = -e$), ions ($q_i = +e$), and grains ($q_d = -Z_d e$), such that $T_e >> T_i, T_d$, respectively. The gravitational inertial force is considered in the ion dynamics to include the full ion-inertial effects. In past, researchers have considered non-isothermal conditions for the inertial fluids in cold plasma system [1, 30, 32]. In their nonlinear evolutionary model, *Verheest et al.* have studied the propagation of electrostatic dust acoustic waves in a uniform gravitating dusty plasma by treating all the constituent species polytropically alike [1, 30]. But, for simplicity now, we here assume both the fluids as isothermal ones with polytropic index of unity ($\Gamma_s = 1$). Thus, equation (8.3) for the isothermal fluids becomes,

$$\frac{\partial M_s}{\partial \tau} + M_s \frac{\partial M_s}{\partial \xi} = -\chi_s \frac{\partial \Phi}{\partial \xi} - \Omega_s \left(\frac{T_s}{T_e}\right) \frac{1}{N_s} \frac{\partial N_s}{\partial \xi} - \frac{\partial \Psi}{\partial \xi} - f_s . \tag{8.4}$$

The spatial distributions of the normalized electrostatic potential (Φ) and the self-gravitational

potential (Ψ) are described by the combining Poisson equations thereby closing the model as,

$$\frac{\partial^2 \Phi}{\partial \xi^2} = -\frac{4\pi e^2}{m_d\, \omega_J^2}\left\{\left(n_{io} N_i - n_{eo} N_e\right) - Z_d\, n_{do} N_d\right\}, \text{ and} \tag{8.5}$$

$$\frac{\partial^2 \Psi}{\partial \xi^2} = \frac{4\pi G m_i n_{io}}{\omega_J^2}\left\{\left(N_i - 1\right) + \alpha\left(\frac{n_{do}}{n_{io}}\right)\left(N_d - 1\right)\right\}. \tag{8.6}$$

Here, n_{io}, and n_{do} model the Jeans swindle [28-29] of the equilibrium unipolar gravitational force field, whereby the self-gravitating inhomogeneous equilibrium is considered as 'homogeneous' on the zeroth-order. The parameter $M_s(\xi)$ represents the flow velocity normalized by the dust sound phase speed (C_{SS}). Electrostatic potential $\Phi(\xi)$ is normalized by the electron thermal potential (T_e/e), and self-gravitational potential $\Psi(\xi)$ is normalized by self-evolving dust acoustic potential (C_{SS}^2). It is clear from equation (8.6) that $\Psi(\xi)$ originates from the inertial force effects jointly contributed by both the cold inertial ions and the cold inertial grains. The independent variables, like position (ξ), and time (τ), are normalized by the Jeans length (λ_J), and Jeans time (ω_J^{-1}) scales, respectively. Moreover, N_e, and N_s are the normalized electron, ion ($s = i$), and grain ($s = d$) densities, normalized by their respective equilibrium values n_{eo}, n_{io}, and n_{do}. In addition, F_{id}, and F_{di} are the ion-dust and dust-ion collision frequencies normalized by the effective Jeans frequency $\omega_J\left(=\sqrt{\omega^2{}_{Ji} + \omega^2{}_{Jd}}\right)$, where $\omega_{Ji} = \sqrt{4\pi G m_i n_{i0}}$, and $\omega_{Jd} = \sqrt{4\pi G m_d n_{d0}}$ are the equilibrium Jeans frequencies due to the gravitating ions and grains, with $G = 6.67408 \times 10^{-11}$ $\mathrm{m^3\ kg^{-1}\ s^{-2}}$ as universal gravitational constant.

8.3.2 Application of Multi-scale Analysis

Before application, here a brief comment is made. The multiscale technique is used to those physical systems, where physical quantities are different on order of magnitude, but are in no way arbitrary [33]. The technique finds approximate solution of a nonlinear complex problem in presence of weak nonlinearity by breaking it in to solvable equilibrium (linear) and perturbation (nonlinear) parts. Application of this technique is fully justifiable in the long evolution time-scale of many weakly nonlinear phenomena, where small modification in the equilibrium can yield large variations in dynamics [33]. We apply this standard methodology [26] over the basic coupled

governing equations in order to study the nonlinear dynamics of low-frequency gravito-electrostatic fluctuations. First, we consider the stretched space and time variables, namely, $X = \in^{1/2} (\xi - \mu\tau)$, and $T = \in^{3/2} \tau$, where μ is the phase velocity (normalized by C_{SS}) of the fluctuations; and $\in$ is a minor order-parameter characterizing the balanced strength of nonlinearity and dispersion [26]. The dependent relevant physical parameters in equations (8.1)-(8.2) and (8.4)-(8.6) are expanded nonlinearly (in various $\in$-powers) around the considered homogeneous equilibrium in perturbational form as follows,

$$\begin{pmatrix} N_e(\xi,\tau) \\ N_s(\xi,\tau) \\ M_s(\xi,\tau) \\ \Phi(\xi,\tau) \\ \Psi(\xi,\tau) \end{pmatrix} = \begin{pmatrix} 1 \\ 1 \\ 0 \\ 0 \\ 0 \end{pmatrix} + \in \begin{pmatrix} N_{e1}(\xi,\tau) \\ N_{s1}(\xi,\tau) \\ M_{s1}(\xi,\tau) \\ \Phi_1(\xi,\tau) \\ \Psi_1(\xi,\tau) \end{pmatrix} + \in^2 \begin{pmatrix} N_{e2}(\xi,\tau) \\ N_{s2}(\xi,\tau) \\ M_{s2}(\xi,\tau) \\ \Phi_2(\xi,\tau) \\ \Psi_2(\xi,\tau) \end{pmatrix} + ... \tag{8.7}$$

It may be noted that gravity-induced space-charge polarization effects may contribute to some finite non-zero values in case of both gravito-electrostatic potentials [34]. But, such gravito-electrostatic polarization effects are neglected here. We now use equation (8.7) in equations (8.1)-(8.2) and (8.4)-(8.6) for order-by-order analyses in accordance with the traditional procedure [26]. Equating the like terms in various powers of $\in$ from both sides of equations (8.1)-(8.2) and (8.4)-(8.6), and applying systematic elimination and substitution procedure, we get the following KdV equation describing the weakly nonlinear electrostatic fluctuations (in terms of Φ_1) on the Jeans scales of space and time, expressed as,

$$\frac{\partial \Phi_1}{\partial T} + A_1 \Phi_1 \frac{\partial \Phi_1}{\partial X} + A_2 \frac{\partial^3 \Phi_1}{\partial X^3} = 0, \tag{8.8}$$

where,

$$A_1 = \left[\frac{n_{eo}}{\mu} + \frac{n_{eo}^2}{n_{io}(\alpha + Z_d)} \left\{ \frac{\alpha}{\mu} \left(\frac{T_i}{T_e} \right) + \mu \right\} \right]^{-1} \left[\begin{array}{l} \dfrac{2 n_{eo}^2 \alpha^2}{n_{io}(\alpha + Z_d)^2} \left\{ 1 - \left(\dfrac{Z_d n_{io}}{n_{do} \alpha^2} \right) \right\} + \\ \dfrac{n_{eo}^3 \alpha}{n_{io}^2 (\alpha + Z_d)^2} \left\{ \left(\dfrac{T_i}{T_e} \right) \alpha - \mu^2 \right\} \end{array} \right], \text{ and} \tag{8.9}$$

$$A_2 = \left[\frac{n_{eo}}{\mu} + \frac{n_{eo}^2}{n_{io}(\alpha + Z_d)} \left\{ \frac{\alpha}{\mu} \left(\frac{T_i}{T_e} \right) + \mu \right\} \right]^{-1} \left[\frac{G m_d^2 n_{do}}{e^2} \left\{ 1 + \frac{1}{\alpha} \left(\frac{n_{io}}{n_{do}} \right) \right\} \right]. \tag{8.10}$$

It is seen analytically from equations (8.9)-(8.10) that both the electrostatic convective coefficient A_1 representing nonlinear wave-steepening effect and electrostatic dispersive coefficient A_2 depicting linear dispersive influence are sensitively dependent on diverse plasma parameters. The analytic constructs of the KdV coefficients are nonlinear and complicated functions of n_{eo}, n_{io}, n_{do}, Z_d, α, T_i/T_e and so forth. It may, however, be an interesting query of readers to know their evolutionary patterns governing the wave propagation dynamics. Thus, the behavior of A_1 and A_2 under the same plasma condition, as discussed in figure 8.2, is described as follows.

(1) For $n_{eo} = 2.43\times10^3$ m^{-3}, 2.53×10^3 m^{-3}, 2.63×10^3 m^{-3}, we obtain $A_1 = 4.85$, 5.05, 5.25 and $A_2 = 6.12\times10^{-1}$, 5.88×10^{-1}, 5.65×10^{-1}; respectively. Thus, as n_{eo} increases, the nonlinear effect (A_1) increases and dispersive effect (A_2) decreases; and vice versa.

(2) For $n_{io} = 1.00\times10^3$ m^{-3}, 1.50×10^3 m^{-3}, 2.00×10^3 m^{-3}, one has $A_1 = 4.85$, 3.23, 2.42 and $A_2 = 6.120\times10^{-1}$, 6.128×10^{-1}, 6.130×10^{-1}; respectively. It shows that, when n_{io} increases, A_1 decreases and A_2 increases; and vice versa.

(3) For $n_{do} = 5.00\times10^{-1}$ m^{-3}, 6.00×10^{-1} m^{-3}, 7.00×10^{-1} m^{-3}, one gets $A_1 = 4.85$ and $A_2 = 6.12\times10^{-1}$, 7.34×10^{-1}, 8.57×10^{-1}; respectively. Thus, as n_{do} increases, A_1 remains the same and A_2 increases; and vice versa.

(4) Further, it is found that there is no sensitive dependence of A_1 and A_2 on Z_d.

(5) For $\alpha = 6.40\times10^{14}$, 6.50×10^{14}, 6.60×10^{14}, one has $A_1 = 4.85$ and $A_2 = 6.12\times10^{-1}$, 6.23×10^{-1}, 6.35×10^{-1}; respectively. Thus, as α increases, A_1 remains the same and A_2 increases; and vice versa.

(6) Lastly, for $T_i/T_e = 1.00\times10^{-3}$, 5.00×10^{-3}, 1.00×10^{-2}, one gets $A_1 = 4.85$, 4.83, 4.80 and $A_2 = 6.12\times10^{-1}$, 6.06×10^{-1}, 5.99×10^{-1}; respectively. Thus, as T_i/T_e increases, both A_1 and A_2 decreases; and vice versa.

Likewise, by applying the same method of elimination and substitution, one gets the following KdV equation for the weakly nonlinear self-gravitational fluctuations (in terms of Ψ_1) on the Jeans scales of space and time,

$$\frac{\partial \Psi_1}{\partial T} + B_1 \Psi_1 \frac{\partial \Psi_1}{\partial X} + B_2 \frac{\partial^3 \Psi_1}{\partial X^3} = 0, \tag{8.11}$$

where,

$$B_1 = \left[\frac{\alpha^2 n_{eo}}{\mu(\alpha + Z_d)(\alpha n_{io} + n_{do})} \left\{ \left(-Z_d - \frac{n_{io}}{n_{do}\alpha}\left(\mu^2 - \frac{T_d}{T_e} \right) \right)^{-1} - \left(\alpha - \frac{\alpha\, n_{eo}}{n_{io}(\alpha + Z_d)} \left(\frac{T_i\,\alpha}{T_e} - \mu^2 \right)^{-1} \right) \right\}^{-1} \right] , \text{ and } \quad (8.12)$$

$$\left[\frac{-2n_{eo}^2 \alpha^2 K_1}{\mu(\alpha + Z_d)(\alpha n_{io} + n_{do})} \left\{ \alpha + \left(\frac{n_{io}}{n_{do}} \right) \right\} \left\{ -\frac{1}{Z_d} - \frac{(T_d - \mu^2 T_e) n_{io} n_{eo}}{Z_d \alpha\, n_{do} \{ T_i\,\alpha - \mu^2 T_e + T_e n_{io}(\alpha + Z_d) \}} \right\} \right]$$

$$B_2 = \left[\frac{\alpha^2 n_{eo}}{\mu(\alpha + Z_d)(\alpha n_{io} + n_{do})} \left\{ \left(-Z_d - \frac{n_{io}}{n_{do}\alpha}\left(\mu^2 - \frac{T_d}{T_e} \right) \right)^{-1} - \left(\alpha - \frac{\alpha\, n_{eo}}{n_{io}(\alpha + Z_d)} \right)^{-1} \left(\frac{T_i\,\alpha}{T_e} - \mu^2 \right) \right\}^{-1} \right] . \quad (8.13)$$

Analytically, again as in the case of electrostatic counterparts, it is evident from equations (8.12)-(8.13) that both the self-gravitational convective coefficient B_1 and self-gravitational dispersive coefficient B_2 sensitively depend on diverse plasma parameters. The evolution of B_1 and B_2 in the same plasma condition, as in figure 8.4, is highlighted as in the following.

(1) For $n_{eo} = 2.50\times10^3$ m^{-3}, 2.60×10^3 m^{-3}, 2.70×10^3 m^{-3}, we obtain $B_1 = 3.20\times10^{-3}$, 3.30×10^{-3}, 3.40×10^{-3} and $B_2 = -2.52$, -2.42, -2.33; respectively. Thus, as n_{eo} increases, B_1 increases and B_2 decreases in magnitude; and vice versa.

(2) For $n_{io} = 1.00\times10^3$ m^{-3}, 1.50×10^3 m^{-3}, 2.00×10^3 m^{-3}, one has $B_1 = 3.20\times10^{-3}$, 2.10×10^{-3}, 1.60×10^{-3} and $B_2 = -2.52$, -3.78, -5.04; respectively. Thus, as n_{io} increases, B_1 decreases and B_2 increases in magnitude; and vice versa.

(3) For $Z_d = 100$, 105, 110, one gets $B_1 = 3.20\times10^{-3}$, 3.00×10^{-3}, 2.90×10^{-3} and $B_2 = -2.52$, -2.64, -2.77; respectively. Thus, as Z_d increases, B_1 decreases and B_2 increases in magnitude; and vice versa.

(4) Lastly, there is no sensitive dependence of B_1 and B_2 on n_{do}, α, T_i/T_e and T_d/T_e.

To see the time-stationary dynamics of the weakly nonlinear gravito-electrostatic eigenmodes, equations (8.8) and (8.11) are transformed into ordinary differential equations by the Galilean co-moving frame transformation, $\rho = X - T$. Thus, equations (8.8) and (8.11) in stationary form are respectively given by,

$$\frac{\partial \Phi_1}{\partial \rho} - A_1 \Phi_1 \frac{\partial \Phi_1}{\partial \rho} - A_2 \frac{\partial^3 \Phi_1}{\partial \rho^3} = 0 \text{, and} \tag{8.14}$$

$$\frac{\partial \Psi_1}{\partial \rho} - B_1 \Psi_1 \frac{\partial \Psi_1}{\partial \rho} - B_2 \frac{\partial^3 \Psi_1}{\partial \rho^3} = 0 . \tag{8.15}$$

Clearly, equations (8.14) and (8.15) together constitute a unique steady-state pair of decoupled KdV equations paving the way for solitary pattern existence in the new spatial coordinate system (defined by ρ). It may be noted that there is no self-consistent source, or sink in the KdV system, unlike previously reported results on the nonlinear evolution of electrostatic dust acoustic waves in a uniform gravitating dusty plasma configuration with all the constituents politropically treated alike [1, 30]. In the latter case, the dust acoustic mode evolution has been found to be governed by the extended KdV equation having a self-consistent nonlocal linear integral sink term arising due to the self-gravitational force field acting on the gravitating massive dust grains. The steady-state analytical solution of equation (8.8), obtained by applying the technique of approximate analytical integration, as used by other authors as well in past [35], can explicitly be written as,

$$\Phi_1 = (\Phi_1)_m \operatorname{sech}^2 \left(\frac{\rho}{\Delta_{ES}} \right), \tag{8.16}$$

where, $(\Phi_1)_m = 3/A_1 \approx 6.18 \times 10^{-1}$ is the amplitude of the electrostatic soliton with average width $\Delta_{ES} = \sqrt{4A_2} \approx 1.56$. The value of convective coefficient $A_1 = 4.85$ and dispersive coefficient $A_2 = 6.12 \times 10^{-1}$ are analytically obtained by using the same plasma parameter values as in figure 8.2. The analytically calculated solitary wave amplitude $(\Phi_1)_m$ exactly matches with that obtained by exact numerical integration (Figure 8.2(a)).

Again, similar to the electrostatic counterparts, the approximate analytical solution of equation (8.11) can be written as,

$$\Psi_1 = (\Psi_1)_m \operatorname{sech}^2 \left(\frac{\rho}{\Delta_{GS}} \right), \tag{8.17}$$

where, $(\Psi_1)_m = 3/B_1 \approx 9.37 \times 10^3$ is the amplitude of the self-gravitational soliton with average width $\Delta_{GS} = \sqrt{4|B_2|} \approx 3.17$. The value of convective coefficient $B_1 = 3.20 \times 10^{-3}$ and dispersive coefficient $B_2 = -2.52$ are analytically obtained by using the same plasma parameter values as used in figure 8.4. The analytically (with approximation of asymptotic behavior) calculated solitary

wave amplitude $(\Psi_1)_m$ shows minor deviation from that obtained by numerical (with no approximation, exact) analysis (Figure 8.4(a)). This shows that there is always some deviation in fluctuation patterns because of the approximate analytical integration in contrast with the exact numerical integration producing the results as shown in figure 8.4(a).

8.3.3 Application of the Sagdeev pseudo-potential Method

In this section, we study the properties of strongly nonlinear (arbitrary amplitude) gravito-electrostatic waves by applying the Sagdeev pseudo-potential approach [27]. Here, we introduce a Galilean frame, $\rho = \xi - \mu\tau$, where μ is the reference frame velocity (normalized by C_{SS}), to obtain the time-stationary form of the governing equations. Applying the appropriate boundary conditions, like $M_d \to 0$, $N_i \to 1$, $\Phi \to 0$, and $\Psi \to 0$ at $\rho \to \pm\infty$ in the stationary frame, equations (8.2) and (8.4)-(8.6) are transformed as,

$$N_i = \frac{1}{1-\left(\frac{-b+\sqrt{b^2-4ac}}{2a\mu}\right)}, \text{ and} \tag{8.18}$$

$$N_d = \frac{1}{1-\left(\frac{-B+\sqrt{B^2-4AC}}{2A\mu}\right)}. \tag{8.19}$$

Now, using N_e, N_i and N_d from equations (8.1), (8.18)-(8.19) in equations (8.5) and (8.6), one gets,

$$\frac{\partial^2\Phi}{\partial\rho^2} = -\frac{4\pi e^2}{m_d\omega_J{}^2}\left[\frac{n_{i0}}{1-\left(\frac{-b+\sqrt{b^2-4ac}}{2a\mu}\right)} - n_{e0}\mathrm{e}^{\Phi} - \frac{n_{d0}\mathrm{Z_d}}{1-\left(\frac{-B+\sqrt{B^2-4AC}}{2A\mu}\right)}\right], \text{ and} \tag{8.20}$$

$$\frac{\partial^2\Psi}{\partial\rho^2} = \frac{m_i n_{i0}}{\rho_0}\left[\left(\frac{1}{1-\left(\frac{-b+\sqrt{b^2-4ac}}{2ac}\right)}-1\right) + \frac{1}{\alpha}\left(\frac{n_{d0}}{n_{i0}}\right)\left(\frac{1}{1-\left(\frac{-B+\sqrt{B^2-4AC}}{2A\mu}\right)}-1\right)\right], \tag{8.21}$$

where,

$$a=\frac{1}{2}\left\{1+\alpha\left(\frac{T_i}{T_e}\right)\left(\frac{1}{\mu^2}\right)\right\},\quad b=\left\{\alpha\left(\frac{T_i}{Te}\right)\left(\frac{1}{\mu}\right)-\mu\right\},\quad c=\alpha\Phi+\Psi+F_{id}\left\{\eta_i\sqrt{\alpha\left(\frac{T_i}{T_e}\right)}-\eta_d\sqrt{\frac{T_d}{T_e}}\right\},$$

$$A=\frac{1}{2}\left\{1+\left(\frac{T_d}{T_e}\right)\left(\frac{1}{\mu^2}\right)\right\},\quad B=\left\{\left(\frac{T_d}{Te}\right)\left(\frac{1}{\mu}\right)-\mu\right\},\text{ and }C=-Z_d\Phi+\Psi+F_{di}\left\{\eta_d\sqrt{\left(\frac{Td}{T_e}\right)}-\eta_i\sqrt{\alpha\left(\frac{T_i}{T_e}\right)}\right\}.$$

Here, $\eta_i=(\rho_i-\rho_{io})$, and $\eta_d=(\rho_d-\rho_{do})$ are defined as the average transit scale-lengths of the ions and the grains, which, typically, are ~ λ_J (Jeans wavelength).

In the electrostatic case, multiplying both sides of equation (8.20) by $\partial\Phi/\partial\rho$ and integrating once under the appropriate boundary conditions, like $\Phi\to 0$ and $\partial\Phi/\partial\rho\to 0$ at $\rho\to\pm\infty$ for localized disturbance, we obtain the energy integral [20, 27, 32, 36] as follows,

$$\frac{1}{2}\left(\frac{\partial\Phi}{\partial\rho}\right)^2+V_E(\Phi,\Psi)=0, \tag{8.22}$$

which describes the energy conservation principle of the electrostatic fluctuation dynamics subjected to the Sagdeev pseudo-potential $V_E(\Phi,\Psi)$ given by

$$V_E(\Phi,\Psi)=\frac{e^2}{\rho_0 m_d G}\left[\begin{array}{l}\frac{1}{\alpha}\mu n_{i0}\left\{\mu-\sqrt{b^2-4ac}-(2a\mu+b)\ln\left\{(2a\mu+b)+\sqrt{b^2-4ac}\right\}\right\}+\\ n_{e0}\left(1-e^{\Phi}\right)+n_{d0}\mu\left\{\mu-\sqrt{B^2-4AC}-(2A\mu+B)\ln\left\{\sqrt{B^2-4AC}\right\}\right\}\end{array}\right]. \tag{8.23}$$

The approximate analytical solution of equation (8.23) in explicit can be obtained by direct integration with inserted integration constant K_E as shown below,

$$\int\left[\left(-\frac{2e^2}{\rho_0 m_d G}\right)\left[\begin{array}{l}\frac{1}{\alpha}\mu^2 n_{i0}+n_{e0}+n_{d0}\mu^2-\frac{1}{\alpha}\mu n_{i0}\left[b_1{}^2-2a_1\{\alpha\Phi+\Psi+F_{id}c_1\}\right]^{1/2}\\ -\frac{1}{\alpha}\mu n_{i0}\left[(a_1\mu+b_1)\ln\left[(a_1\mu+b_1)+\left[b_1{}^2-2a_1\{\alpha\Phi+\Psi+c_1\}\right]^{1/2}\right]\right]\\ -n_{e0}e^{\Phi}-n_{d0}\mu\left[b_2{}^2-2a_2\{-Z_d\Phi+\Psi+F_{di}c_2\}\right]^{1/2}-\\ n_{d0}\mu(a_2\mu+b_2)\ln\left[(a_2\mu+b_2)+\left[b_2{}^2-2a_2\{\alpha\Phi+\Psi+c_2\}\right]^{1/2}\right]\end{array}\right]\right]^{-1/2}d\Phi=\rho+K_E, \tag{8.24}$$

It is clearly seen that the mathematical construct of equation (8.24) is highly complicated and nonlinear in nature. So, derivation of analytical (approximate) solutions is skipped here in order for having numerical (exact) results presented later. Differentiating equation (8.23) successively with respect to Φ, one gets

$$\frac{\partial V_E(\Phi,\Psi)}{\partial \Phi} = \frac{4\pi e^2}{m_d \omega_J{}^2}\left[\frac{n_{i0}}{1-\left(\frac{-b+\sqrt{b^2-4ac}}{2a\mu}\right)} - n_{e0}\mathrm{e}^{\Phi} - \frac{n_{d0}\,\mathrm{Z_d}}{1-\left(\frac{-B+\sqrt{B^2-4AC})}{2A\mu}\right)}\right], \tag{8.25}$$

$$\frac{\partial^2 V_E(\Phi,\Psi)}{\partial \Phi^2} = -\frac{4\pi e^2}{m_d \omega_J{}^2}\left[\frac{n_{i0}\alpha\left(b^2-4ac\right)^{-1/2}}{\mu\left\{1-\left(\frac{-b+\sqrt{b^2-4ac}}{2a\mu}\right)\right\}^2} + n_{e0}\,\mathrm{e}^{\Phi} + \frac{n_{d0}\,\mathrm{Z_d^2}\left(B^2-4AC\right)^{-1/2}}{\mu\left\{1-\left(\frac{-B+\sqrt{B^2-4AC}}{2A\mu}\right)\right\}^2}\right], \text{ and} \tag{8.26}$$

$$\frac{\partial^3 V_E(\Phi,\Psi)}{\partial \Phi^3} = -\frac{4\pi e^2}{m_d \omega_J{}^2}\left[\begin{array}{l}\dfrac{2n_{i0}\alpha^2}{\left\{1-\left(\frac{-b+\sqrt{b^2-4ac}}{2a\mu}\right)\right\}^3}\left[\left\{1-\left(\frac{-b+\sqrt{b^2-4ac}}{2a\mu}\right)\right\}a\left(b^2-4ac\right)^{-3/2} - \dfrac{2\left(b^2-4ac\right)^{-1}}{\mu}\left(b^2-4ac\right)^{-1/2}\right] + \\ n_{e0}\,\mathrm{e}^{\Phi} + \dfrac{2n_{d0}\,\mathrm{Z_d^3}}{\left\{1-\left(\frac{-B+\sqrt{B^2-4AC}}{2A\mu}\right)\right\}^3}\left[\left(-A\right)\left(B^2-4AC\right)^{-3/2}\left\{1-\left(\frac{-B+\sqrt{B^2-4AC}}{2A\mu}\right)\right\} + \dfrac{\left(B^2-4AC\right)^{-1}}{\mu}\right]\end{array}\right]. \tag{8.27}$$

We now carry out prerequisite analytical tests to check the conditions for the existence of solitary structures and their qualitative properties governed by equation (8.22). It is found that equations (8.23), (8.25)-(8.27) under cold plasma condition, $T_s/T_e \sim 0$ [36], satisfies the following extreme conditions meant for the existence of compressive soliton-like patterns [20, 27, 32, 36] as follows,

$$\left.\begin{aligned}
&V_E(\Phi,\Psi)=0,\ \frac{\partial V_E(\Phi,\Psi)}{\partial\Phi}=0,\quad \text{at } \Phi=0,\ \Psi=0,\\
&\frac{\partial^2 V_E(\Phi,\Psi)}{\partial\Phi^2}<0,\quad \text{at } \Phi=0,\ \Psi=0,\\
&\frac{\partial^3 V_E(\Phi,\Psi)}{\partial\Phi^3}>0,\ \text{at } \Phi=0,\ \Psi=0,\\
&V_E(\Phi,\Psi)=0,\ \text{at } \Phi=\Phi_{\max},\ \text{and}\\
&V_E(\Phi,\Psi)<0\ \text{ for } 0<|\Phi|<|\Phi_{\max}|.
\end{aligned}\right\} \tag{8.28}$$

In equation (8.28), it is seen that $\partial^3 V_E(\Phi,\Psi)/\partial\Phi^3>0$ at $\Phi=0$, $\Psi=0$, which is the condition for existence of compressive solitonic structures [32]. So, the analytical examination shows the evolutionary possibility for compressive solitary patterns.

For the self-gravitational counterparts, we multiply equation (8.21) by $\partial\Psi/\partial\rho$ and integrate once with appropriate boundary conditions, like $\Psi\to 0$ and $\partial\Psi/\partial\rho\to 0$ at $\rho\to\pm\infty$ for localized disturbance. Thus, the self-gravitational energy integral equation is obtained as follows,

$$\frac{1}{2}\left(\frac{\partial\Psi}{\partial\rho}\right)^2+V_G(\Phi,\Psi)=0, \tag{8.29}$$

which depicts the energy conservation law of the self-gravitational fluctuation dynamics subjected to the self-gravitational Sagdeev pseudo-potential $V_G(\Phi,\Psi)$ described as,

$$V_G(\Phi,\Psi)=\frac{m_i n_{io}}{\rho_0}\left[\begin{aligned}
&-\left(\mu\sqrt{b^2-4ac}\right)+(2a\mu+b)\mu\ln\left\{(2a\mu+b)+\sqrt{b^2-4ac}\right\}-\Psi+\frac{1}{\alpha}\left(\frac{n_{d0}}{n_{i0}}\right)\\
&\left\{-\mu\sqrt{B^2-4AC}+(2A\mu+B)\mu\ln\left\{(2A\mu+B)+\sqrt{B^2-4AC}\right\}-\Psi\right\}
\end{aligned}\right]. \tag{8.30}$$

Now, the approximate analytical solution of equation (8.30) can also be derived by direct integration with integration constant K_G as in the following,

$$\int\left[\left(-\frac{2m_i n_{io}}{\rho_0}\right)\left[\begin{aligned}
&-\mu\left[b_1{}^2-2a_1\{\alpha\Phi+\Psi+F_{id}c_1\}\right]^{1/2}-\Psi+(a_1\mu+b_1)\mu\\
&\ln\left[(a_1\mu+b_1)+\left[b_1{}^2-2a_1\{\alpha\Phi+\Psi+c_1\}\right]^{1/2}\right]-\frac{1}{\alpha}\left(\frac{n_{d0}}{n_{i0}}\right)\mu\\
&\left[b_2{}^2-2a_2\{-Z_d\Phi+\Psi+F_{di}c_2\}\right]^{1/2}+\frac{1}{\alpha}\left(\frac{n_{d0}}{n_{i0}}\right)\\
&\left[\mu(a_2\mu+b_2)\ln\left[(a_2\mu+b_2)+\left[\begin{matrix}b_2{}^2-2a_2\\ \{-Z_d\Phi+\Psi+F_{di}c_2\}\end{matrix}\right]^{1/2}\right]-\Psi\right]
\end{aligned}\right]\right]^{-1/2} d\Psi=\rho+K_G. \tag{8.31}$$

As in the case of electrostatic formalism, here too, the mathematical structure of equation (8.31) is highly complicated and nonlinear in shape, which is therefore skipped here in order for obtaining exact numerical solutions presented later. Now, differentiating equation (8.29) successively with respect to Ψ, one gets

$$\frac{\partial V_G(\Phi,\Psi)}{\partial \Psi} = -\frac{m_i n_{i0}}{\rho_0}\left[\left(\frac{1}{1-\left(\frac{-b+\sqrt{b^2-4ac}}{2ac}\right)}-1\right)+\frac{1}{\alpha}\left(\frac{n_{d0}}{n_{i0}}\right)\left(\frac{1}{1-\left(\frac{-B+\sqrt{B^2-4AC}}{2A\mu}\right)}-1\right)\right], \tag{8.32}$$

$$\frac{\partial^2 V_G(\Phi,\Psi)}{\partial \Psi^2} = -\frac{m_i n_{i0}}{\rho_0 \mu}\left[-\frac{\alpha\left(b^2-4ac\right)^{-1/2}}{\left\{1-\left(\frac{-b+\sqrt{b^2-4ac}}{2ac}\right)\right\}^2}+\frac{1}{\alpha}\left(\frac{n_{d0}}{n_{i0}}\right)\frac{Z_d\left(B^2-4AC\right)^{-1/2}}{\left\{1-\left(\frac{-B+\sqrt{B^2-4AC}}{2A\mu}\right)\right\}^2}\right], \text{ and} \tag{8.33}$$

$$\frac{\partial^3 V_G(\Phi,\Psi)}{\partial \Psi^3} = -\frac{m_i n_{i0}}{\rho_0 \mu}\left[\begin{array}{l} -\dfrac{2\alpha^2}{\left\{1-\left(\frac{-b+\sqrt{b^2-4ac}}{2ac}\right)\right\}^3}\left[\left\{1-\left(\frac{-b+\sqrt{b^2-4ac}}{2ac}\right)\right\}a\left(b^2-4ac\right)^{-3/2}\right. \\ \left.\qquad -\dfrac{1}{\left(b^2-4ac\right)}\right] \\ +\dfrac{1}{\alpha}\left(\dfrac{n_{d0}}{n_{i0}}\right)\dfrac{2Z_d^2}{\left\{1-\left(\frac{-B+\sqrt{B^2-4AC}}{2A\mu}\right)\right\}^3}\left[\left\{1-\left(\dfrac{-B+\sqrt{B^2-4AC}}{2A\mu}\right)\right\}\right. \\ \left.\left\{-\dfrac{A}{\left(B^2-4AC\right)^{3/2}}\right\}+\dfrac{1}{\mu\left(B^2-4ACc\right)}\right] \end{array}\right]. \tag{8.34}$$

It is analytically verified that equations (8.30), (8.32)-(8.34) satisfy the following conditions predicting the dynamical evolution of possible self-gravitational rarefactive soliton-like patterns [20, 27, 32, 36] as follows,

$$\left.\begin{aligned}
&V_G(\Phi,\Psi)=0,\ \frac{\partial V_G(\Phi,\Psi)}{\partial \Psi}=0, \quad \text{at } \Phi=0,\ \Psi=0,\\
&\frac{\partial^2 V_G(\Phi,\Psi)}{\partial \Psi^2}<0, \quad \text{at } \Phi=0,\ \Psi=0,\\
&\frac{\partial^3 V_G(\Phi,\Psi)}{\partial \Psi^3}>0, \text{ at } \Phi=0,\ \Psi=0,\\
&V_G(\Phi,\Psi)=0 \text{ , at } \Psi=\Psi_{\max}, \text{ and}\\
&V_G(\Phi,\Psi)<0 \text{ for } 0<|\Psi|<|\Psi_{\max}|.
\end{aligned}\right\} \tag{8.35}$$

In equation (8.35), it is found that $\partial^3 V_G(\Phi,\Psi)/\partial\Psi^3<0$ at $\Phi=0$, $\Psi=0$, which is the condition for existence of rarefactive solitonic structures [32]. As in the electrostatic fluctuations, the analytical inspection of existential conditions for the self-gravitational fluctuations shows the growth possibility for rarefactive soliton-like structures.

It may be seen that the conditions for existence of compressive soliton-like structures are $\partial^3 V_E(\Phi,\Psi)/\partial\Phi^3>0$, $\partial^3 V_G(\Phi,\Psi)/\partial\Psi^3>0$ at $\Phi=0$, $\Psi=0$, whereas, for rarefactive soliton-like patterns, the same are $\partial^3 V_E(\Phi,\Psi)/\partial\Phi^3<0$, $\partial^3 V_G(\Phi,\Psi)/\partial\Psi^3<0$ [32]. For exact characterization of the wave spectrum with these basic inputs kept in mind, equations (8.22) and (8.29) numerically integrated by the RK-IV method as discussed in the next section.

8.4 RESULTS AND DISCUSSIONS

An evolutionary sound calculation scheme to explore the properties of both weakly and strongly nonlinear gravito-electrostatic fluctuation dynamics supported in unmagnetized, inhomogeneous, collisional DMC of infinite extension is proposed. It self-consistently considers the frictional dynamics of the ions and grains in presence of the non-static ion-inertial response effects. It is analytically shown that weakly nonlinear gravito-electrostatic eigenmode evolutions are expressible by a unique pair of decoupled KdV equations (equations (8.8) and (8.11)) obtained by multiscale analyses. On the other hand, the fully nonlinear complements are governed by an idiosyncratic pair of coupled energy integral equations (equations (8.22) and (8.29)) derived by implementing the Sagdeev pseudo-potential methodology. The governing equations for both the distinctive classes (weakly and strongly nonlinear) of fluctuations are integrated numerically as initial value problems in a time-stationary configuration (RK-IV) followed by spatiotemporal

analysis (FD) as already mentioned above. The numerical results are presented in two subsections, one for the weakly nonlinear and the other for strongly nonlinear fluctuations, as follows.

8.4.1 Weakly Nonlinear Fluctuations

The obtained profiles on the weak fluctuations (both spatial and spatiotemporal) with a suitable wide-range choice of judicious plasma-parameters values are discussed below.

Figure 8.2 presents the spatial profile of the normalized lowest-order perturbed electrostatic (a) potential, (b) field, (c) potential curvature, and (d) phase portrait. Various lines now correspond to Case (1): $n_{io} = 1.00 \times 10^3$ m^{-3} (blue line), Case (2): $n_{io} = 1.10 \times 10^3$ m^{-3} (red line), Case (3): $n_{io} = 1.20 \times 10^3$ m^{-3} (green line), and Case (4): $n_{io} = 1.30 \times 10^3$ m^{-3} (black line), respectively. Different input initial values used are $(\Phi)_i = 1.00 \times 10^{-3}$, $(\Phi_\rho)_i = -1.00 \times 10^{-4}$, and $(\Phi_{\rho\rho})_i = 1.50 \times 10^{-2}$. The other parameters kept fixed are $Z_d = 100$, $n_{eo} = 2.43 \times 10^3$ m^{-3}, $m_d = 1.07 \times 10^{-12}$ kg, $n_{do} = 5.00 \times 10^{-1}$ m^{-3} and $\mu = 1.00$ [1-2, 5, 15, 21, 36]. The potential fluctuations (Figure 8.2(a)) show compressive soliton-like eigenmodes, which are in qualitatively good correspondence with those as obtained by others in different situations [11, 16-19, 24]. It is observed that when n_{io} increases, the amplitude of corresponding potential fluctuations also increases with increment in the ion-inertial effect. Physically, it may happen for the following collective processes: (i) Due to the ion-inertial effects, increasing n_{io} creates more deviation from the quasi-neutrality condition by weakening the ion-electron-dust sticking mechanism. Thus, the electrostatic repulsive pressure among the charged particles increases against the self-gravitational attractive pressure, thereby contributing to the amplitude-growth. (ii) In presence of the dynamic ion-inertial response, increasing n_{io} contributes to the increased self-gravitational field effects, thereby enhancing the strength of gravity-induced space-charge polarization [34] resulting in increasing the electrostatic fluctuation amplitude. The electric field (Figure 8.2(b)) and curvature (Figure 8.2(c)) profiles evolve as a mixture of rarefactive and compressive soliton; and bell-shaped soliton-like structures, respectively. Lastly, Figure 8.2(d) shows the phase portrait in the phase space defined by Φ_1 and $\Phi_{1\rho}$, which gives a parametric representation of the geometrical trajectories for the global behavior of the local fluctuations. It shows that with increase in n_{io}, the stability of the cloud is highly disturbed as we go away from the center. This is because of the fact that the trajectories of the

phase portraits get separated from one another as the perturbed potential increases from the center outwards. The evolutionary profiles of the weakly nonlinear electrostatic fluctuations due to other sensitive plasma parameter variations (such as m_d, n_{do}, and n_{eo}) are shown and discussed elaborately in Ref. [37].

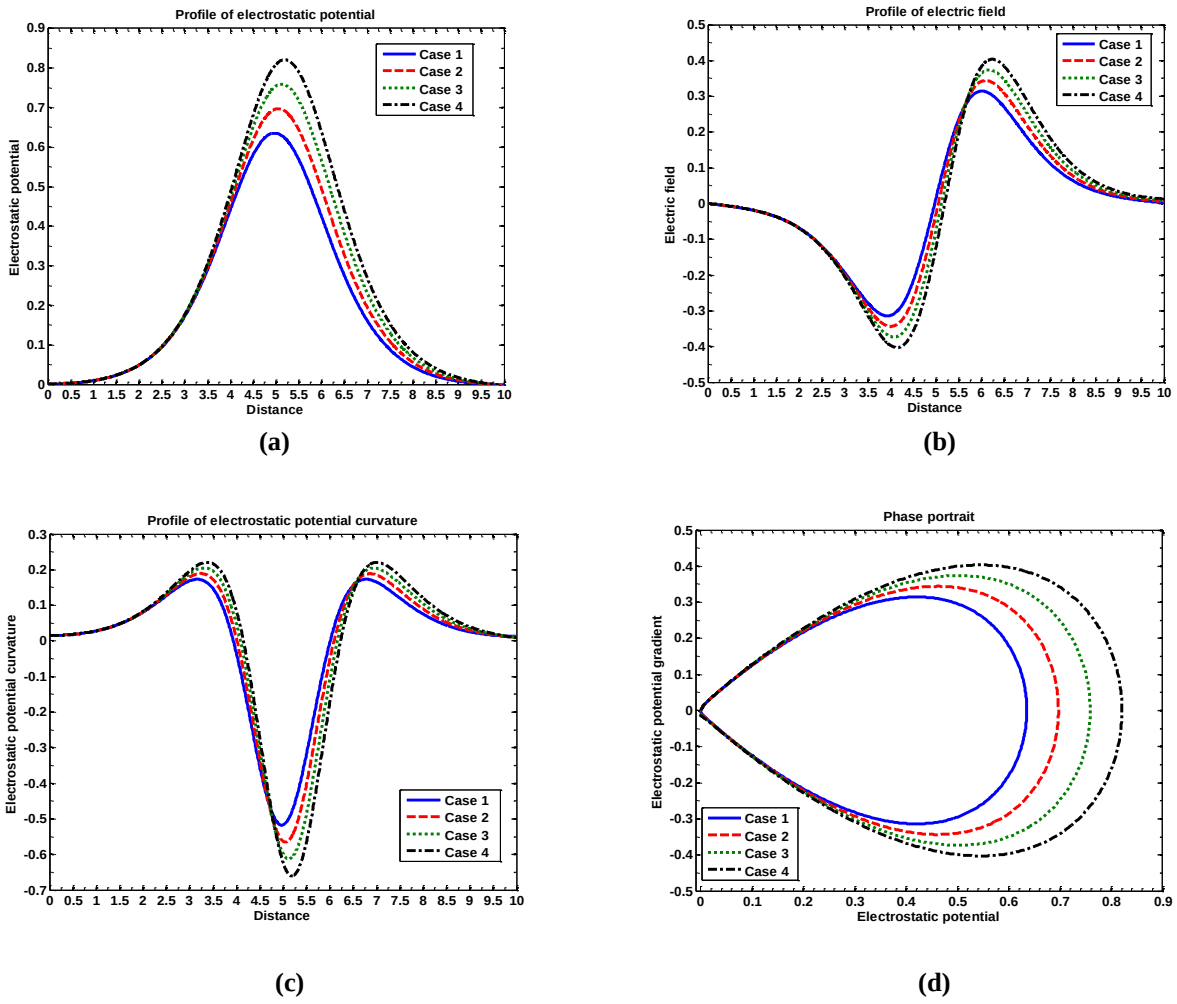

Figure 8.2 *Spatial profile of the normalized lowest-order perturbed electrostatic (a) potential, (b) field, (c) potential curvature, and (d) phase portrait. Various lines correspond to Case (1):* $n_{io} = 1.00 \times 10^3$ m^{-3} *(blue line), Case (2):* $n_{io} = 1.10 \times 10^3$ m^{-3} *(red line), Case (3):* $n_{io} = 1.20 \times 10^3$ m^{-3} *(green line), and Case (4):* $n_{io} = 1.30 \times 10^3$ m^{-3} *(black line), respectively. Various input and initial parameter values are shown in the text.*

For the spatiotemporal evolution, equation (8.8) is integrated by the FD under suitable boundary conditions as discussed above. Figure 8.3 depicts the perturbed potential evolving in the

astrophysical space and time under the same conditions as figure 8.2, but now with the numerically fitted initial value, $(\Phi_1)_{xi} = 0.66\,\mathrm{sec}\,h\{(x^{1.4} - 10)\}$. The boundary conditions applied here are: (i) densities and dust-charge at infinity are asymptotically zero, (ii) velocities at the cloud center are zero, and (iii) potentials at the center and asymptotically at infinity are zero. The snapshot of figure 8.3 is same in magnitude and structure as in figure 8.2. It reflects the basic normal feature of solitary structures as temporally stable ones.

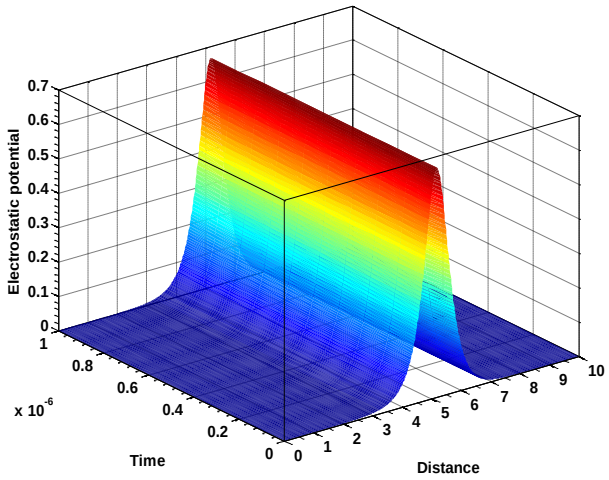

Figure 8.3 *Spatiotemporal profile of the normalized lowest-order perturbed electrostatic potential under the same condition as figure 8.2. The boundary conditions and input initial values are presented in the text.*

The physical strength of the potential fluctuations (Figure 8.2(a)) for average normalized value $\Phi_1 \sim 6.25\times10^{-1}$ is estimated as, $\Phi_{phys} \sim \in (T_e \Phi_1 / e) \sim 10^{-3}$ V, in the HII region with $\in = 10^{-2}$ and $T_e = 10^4$ K [1-2, 5, 15, 21, 36]. The fluctuation wave amplitude is maximum at $\rho = 5\lambda_J$. The field fluctuations (Figure 8.2(b)) evolve with amplitudes having average normalized value $\sim 4\times10^{-1}$, which is physically calculated as, $E_{phys} \sim \in (T_P E_{e1} / e\lambda_J) \sim 4.00\times10^{-11}$ V m^{-1}. The curvature profile (Figure 8.2(c)) exhibits bell-shaped solitary eigenmodes. The degree of deviation from the cloud quasi-neutrality is not uniform in presence of the gravitating ions; it shows noticeable variation for $3\lambda_J < \rho < 7.5\lambda_J$ with maximum at $\rho = 5\lambda_J \sim 5\times10^8$ m. The average curvature fluctuation strength is calculated as, $(\partial_{xx}\Phi)_{phys} \sim \in (T_p \partial_{\rho\rho} \Phi_1 / e\lambda_J^2) \sim 2.00\times10^{-19}$ V m^{-2}, which is very small (~0).

This signifies that the cloud quasi-neutrality is not affected appreciably due to the considered weakly nonlinear (<3rd order) perturbation.

Let us now describe the self-gravitational fluctuation dynamics governed by the KdV equation, equation (8.11). The dynamics is contributed jointly by the inertial dust grains and inertial ions. To obtain the detailed features, the system is integrated numerically as before. The resulting profiles are descriptively presented in figures 8.4-8.5 as the following.

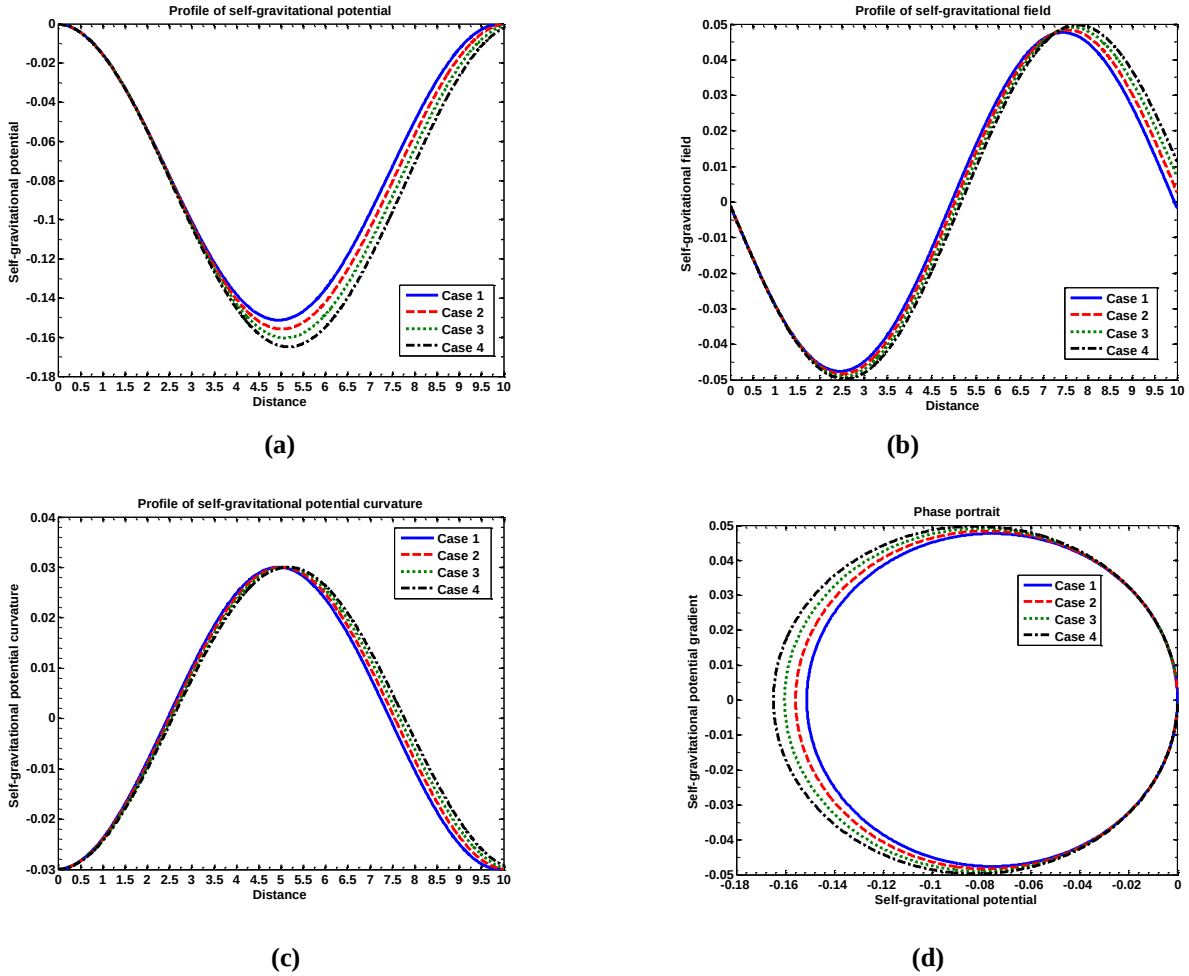

Figure 8.4 *Spatial profile of the normalized lowest-order perturbed self-gravitational (a) potential, (b) field, (c) potential curvature, and (d) phase portrait. Various lines correspond to Case (1):* $n_{io} = 1.00 \times 10^3$ m^{-3} *(blue line), Case (2):* $n_{io} = 1.03 \times 10^3$ m^{-3} *(red line), Case (3):* $n_{io} = 1.06 \times 10^3$ m^{-3} *(green line), and Case (4):* $n_{io} = 1.09 \times 10^3$ m^{-3} *(black line), respectively. Various input and initial parameter values are given in the text.*

Figure 8.4 graphically shows spatial profiles of the normalized lowest-order perturbed self-gravitational (a) potential, (b) field, (c) potential curvature, and (d) phase portrait. Various lines correspond to Case (1): $n_{io} = 1.00 \times 10^3$ m^{-3} (blue line), Case (2): $n_{io} = 1.03 \times 10^3$ m^{-3} (red line), Case (3): $n_{io} = 1.06 \times 10^3$ m^{-3} (green line), and Case (4): $n_{io} = 1.09 \times 10^3$ m^{-3} (black line), respectively. Different input initial values used are $(\Psi)_i = -1.00 \times 10^{-4}$, $(\Psi_\rho)_i = -1.00 \times 10^{-3}$, and $(\Psi_{\rho\rho})_i = -3.00 \times 10^{-2}$. The other parameters kept fixed are $Z_d = 100$, $\mu = 0.06$, $n_{eo} = 2.50 \times 10^3$ m^{-3}, $n_{do} = 1.00 \times 10^{-1}$ m^{-3} and $m_d = 1.07 \times 10^{-12}$ kg. The potential fluctuations evolve as bell-shaped soliton-like structures (Figure 8.4(a)), the amplitude of which increases with increase in n_{io}. As n_{io} increases, the self-gravitational effects increase in presence of the gravitating ions. As a consequence, the self-gravitational fluctuation increases. It provides strong evidence in support of the fact that the consideration of ion-inertia has effective contribution in the propagation and excitation of nonlinear eigenmodes. The corresponding field (Figure 8.4(b)) and curvature (Figure 8.4(c)) fluctuations evolve as mixtures of rarefactive and compressive soliton-like; and compressive soliton-like structures, respectively. The phase portrait (Figure 8.4(d)) gives the geometrical trajectories of the inertial species in the phase plane of Ψ_1 and $\Psi_{1\rho}$. The trajectories show closed structures revealing that the DMC fluctuations form a conservative system. The evolutionary profiles of the weakly nonlinear self-gravitational fluctuations due to other sensitive plasma parameter variations (such as Z_d, and n_{eo}) are elaborately discussed in Ref. [37].

To obtain the 3-D spatiotemporal profiles, equation (8.11) is integrated as before. The self-gravitational fluctuation is shown in figure 8.5. The conditions are the same as figure 8.4, but with a numerically fitted initial potential value, $(\Psi_1)_{xi} = 0.14 \mathrm{sec}h\{(x^{1.4} - 10)\}$. The magnitude and structure of this profile sketch is the same as those of the time-stationary ones (Figure 8.4).

The physical strength of the potential fluctuations for average normalized value $\Psi_1 \sim |1.6 \times 10^{-1}|$ is estimated as, $|\Psi_{phys}| \sim \in (C_{SS}^2 \Psi_1) \sim 2.24 \times 10^{-11}$ J kg^{-1}, in the HII region with $\in = 10^{-2}$ and $C_{SS}^2 \sim 1.4 \times 10^{-7}$ J kg^{-1} [1-2, 5, 15, 21, 36]. The fluctuations for all the conditions found to be maximum at $\rho = 5\lambda_J \sim 5 \times 10^8$ m. The field fluctuations (Figure 8.4(b)) evolve as mixtures of rarefactive and compressive soliton-like spectral patterns with average amplitude,

$\left|E_{gphys}\right| \sim \in \left(E_{g1}C_{SS}^2/\lambda_J\right) \sim 7.00\times10^{-19}$ J kg^{-1} m^{-1}. The curvatures (Figure 8.4(c)) exhibit compressive solitary anatomical structures having average strength found as, $\left(\partial_{xx}\Psi\right)_{phys} \sim \in \left(\partial_{\rho\rho}\Psi_1 C_{SS}^2/\lambda_J^2\right)$ $\sim 4.20\times10^{-28}$ J kg^{-1} m^{-2}, which is very small (~0) owing to weak nonlinearly (<3rd order) taken into account. Thus, the cloud inertial mass-neutrality, although the active ion-inertial dynamics is taken into account, is not appreciably affected in the weak disturbance analysis.

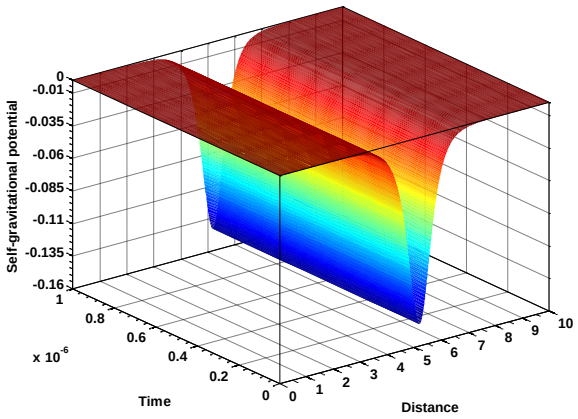

Figure 8.5 *Spatiotemporal profile of the normalized lowest-order perturbed self-gravitational potential under the same condition as figure 8.4. The boundary conditions and input values are presented in the text.*

In comparison, we see that the strength of the self-gravitational fluctuations is weaker than the electrostatic counterparts ($\Phi_1/\Psi_1 \approx 3.8$). The phase portraits of both the Coulombic (Figure 8.2(d)) and Newtonian (Figure 8.4(d)) species reveal a conservative dynamical system, since the trajectories evolve as closed-form structures. For increasing (decreasing) different plasma parameters, the trajectories overlap over one another at the potential value corresponding to that near the cloud center. Therefore, it is pertinent to add that the central portion of the cloud surrounds the most stable fixed point. The trajectories in the phase portraits start to get slightly separated from one another as the perturbed potential increases (decreases) in magnitude from the center of the cloud outwards. The dusty cloud thus gets gradually more unstable at spatial points away from the center of the cloud.

8.4.2 Strongly Nonlinear Fluctuations

To study the dynamical characteristics of the strongly nonlinear (arbitrary amplitude) gravito-electrostatic fluctuations, we numerically solve electrostatic (8.22) and self-gravitational equation

(8.29), as already highlighted in the text. It is, as already examined analytically too, seen that both the distinct families of the Sagdeev potential profiles graphically support the evolutionary criterion for solitary eigenmode patterns. It is noticeable that the corresponding physical potentials for electrostatic and self-gravitational fluctuations evolve as compressive and rarefactive soliton-like structures, respectively. The detailed characteristic features of the numerical results are, in an elaborate way, discussed as follows.

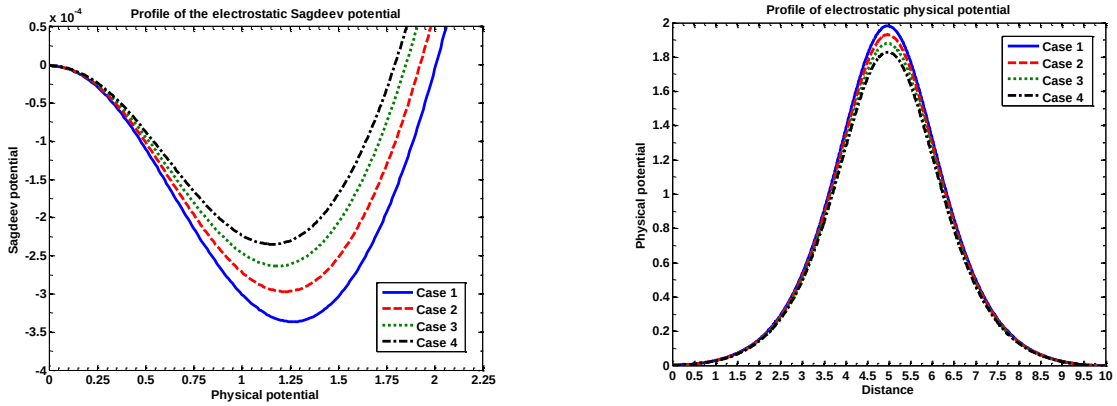

(a) **(b)**

Figure 8.6 *Spatial profile of the normalized electrostatic (a) Sagdeev potential, and (b) physical potential. Various lines correspond to Case (1):* $m_d = 4.00 \times 10^{-12}$ *kg (blue line), Case (2):* $m_d = 4.30 \times 10^{-12}$ *kg (red line), Case (3):* $m_d = 4.60 \times 10^{-12}$ *kg (green line), and Case (4):* $m_d = 4.90 \times 10^{-12}$ *kg (black line), respectively. Various input and initial parameter values are presented in the text.*

Figure 8.6 graphically portrays the electro-dynamical evolution of the normalized electrostatic (a) Sagdeev potential, and (b) physical potential. Various lines now stand for Case (1): $m_d = 4.00 \times 10^{-12}$ kg (blue line), Case (2): $m_d = 4.30 \times 10^{-12}$ kg (red line), Case (3): $m_d = 4.60 \times 10^{-12}$ kg (green line), and Case (4): $m_d = 4.90 \times 10^{-12}$ kg (black line), respectively. The other parameters kept fixed are $Z_d = 100$, $n_{io} = 7.00 \times 10^7$ m^{-3}, $n_{do} = 5.00 \times 10^2$ m^{-3}, $n_{eo} = 1.00 \times 10^7$ m^{-3}, $F_{id} = 1.00 \times 10^{-4}$ and $\mu = 1.00$. The Sagdeev potential (Figure 8.6(a)) shows solitary eigenmodes, which satisfies all the analytical conditions pre-tested for the existence of solitary solutions. The physical potential (Figure 8.6(b)) evolves as compressive soliton-like structures corresponding to the Sagdeev potential (Figure 8.6(a)). In both the Sagdeev and physical potentials, the amplitude of the eigenmodes decreases with increasing m_d. The basic physical

insight underlying this is that with the increase in m_d, the self-gravitational effect of the cloud increases, which dominates the wave amplitude of the electrostatic fluctuations counterpart. It is interesting to note that for $10^{-13} < m_d < 10^{-10}$ kg, the compressional solitary structures are supported in our cloud model. The detail of other numerical evolutionary profiles by varying n_{eo}, and n_{do} are shown in Ref. [37].

In parallel way, figure 8.7 presents evolutionary profiles of the self-gravitational (a) Sagdeev potential, and (b) physical potential. Various lines now take after Case (1): $n_{io} = 6.00 \times 10^4$ m^{-3} (blue line), Case (2): $n_{io} = 6.30 \times 10^4$ m^{-3} (red line), Case (3): $n_{io} = 6.60 \times 10^4$ m^{-3} (green line), and Case (4): $n_{io} = 6.90 \times 10^4$ m^{-3} (black line), respectively. The other parameters kept fixed are $Z_d = 110$, $n_{do} = 1.00 \times 10^1$ m^{-3} $m_d = 4.00 \times 10^{-12}$ kg, $F_{id} = 1.00 \times 10^{-4}$ and $\mu = 1.00$. Here, as already confirmed analytically before, it is found that the Sagdeev potential (Figure 8.7(a)) satisfies the requisite criterion, thereby allowing the real potential to evolve rarefactive solitary waves (Figure 8.7(b)) for $10^4 < n_{io} < 10^6$ m^{-3}. The basic mechanism is the same as in figure 8.4. It is also seen that the solitary amplitude increases with increasing n_{do} in the range $10^{-1} < n_{do} < 10^3$ m^{-3} (figure in Ref. [37]). The amplitude-growth is attributable to the ion-inertial effects and the dust-inertial effects within the classical limit of the Newtonian dynamics.

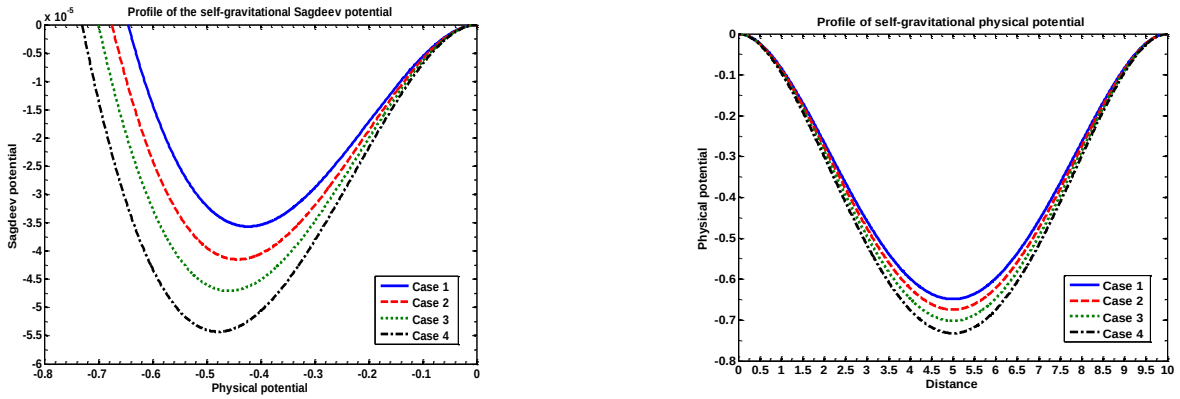

(a) **(b)**

Figure 8.7 *Spatial profile of the normalized self-gravitational (a) Sagdeev potential and (b) physical potential. Various lines correspond to Case (1):* $n_{io} = 6.00 \times 10^4$ *m*$^{-3}$ *(blue line), Case (2):* $n_{io} = 6.30 \times 10^4$ *m*$^{-3}$ *(red line), Case (3):* $n_{io} = 6.60 \times 10^4$ *m*$^{-3}$ *(green line), and Case (4):* $n_{io} = 6.90 \times 10^4$ *m*$^{-3}$ *(black line), respectively. Various input and initial parameter values are presented in the text.*

The physical strength of the strongly nonlinear electrostatic potential for the average normalized potential $\Phi_N \sim 2.00$ is calculated as, $\Phi_p \sim 2.00$ V, in the HII region with $T_e \sim 10^4$ K [1-2, 5, 15, 21, 36]. Similarly, the physical value of self-gravitational potential is figured as, $\Psi_p \sim 1.12 \times 10^{-9}$ J kg^{-1}, for the average normalized potential, $\Psi_N \sim 8.00 \times 10^{-1}$. Thus, in the considered nonlinear regimes and in the typical plasma parameter domains, the electrostatic repulsive potential overcomes the self-gravitational attractive counterpart in both the cases of weak nonlinearity ($\Phi_1/\Psi_1 \approx 3.8$) and strong nonlinearity ($\Phi_N/\Psi_N \approx 2.5$).This implies that enhanced self-gravity effects by very massive dense grains are required for equilibrium bounded structure formation via gravito-electrostatic interplay mechanism. This lacuna might be due to the neutral fluid dynamics frictionally coupled with the collapsing plasma mass via self-gravity missed in our analysis.

In comparison, the stability analysis presented here, with the effective ion-inertial contribution accounted in totality, differs from the existing weakly [11, 23, 30, 38-40] and strongly [20, 41] nonlinear analyses in fundamentality as well as in observation. The main differences in the light of the available reports are summarily presented in Table 8.1 as follows.

Table 8.1: Comparison between our model and existing model analyses

No	Items	Our analysis	Existing analyses
1	Type of plasma	Cold dusty plasma with the inertial ions in presence of self-gravity ($T_d, T_i << T_e$)	Cold plasma with only thermal ions, excluding inertial ions $\left(T_d << T_i \approx T_e = T_p\right)$ [11, 23, 30, 38-40]
2	Dynamic ion-inertial response effects	Included	Not included [1, 30, 40]
3	Collisions between the ions and dust	Considered	Neglected [11, 23, 30, 38-40]
4	Equation of state	Polytropic (special case of the inertial ions and grains considered)	Polytropic state of all the plasma constituent species [1, 30]

5	Self-gravity perturbative correction	First order (lowest-order)	Second order (higher-order) [1, 30]
6	Normalization and scale-invariance schemes	Standard astrophysical normalization procedure done on the Jeans scales of space and time	Not done [11, 23, 30, 38-40]
7	Jeans swindle	Applied	Neglected for considered entire uniformity [11, 23, 30, 38-40]
8	Eigenmode equation (weak nonlinearity)	Paired decoupled KdV equations	Paired Coupled KdV [11, 23], Extended KdV [30] , decoupled KdV [38], KdV [40] equations
9	Existence of self-consistent source or sink	No source or sink in the decoupled KdV system due to non-static response of the gravitating ions	Nonlocal linear integral sink in the extended KdV equation, due to the gravitating dust amid the plasma constituents polytropically treated alike [1, 30]
10	Eigenmode structures (weak nonlinearity)	Solitary spectral patterns, electrostatic compressive and self-gravitational rarefactive solitons	Soliton-like modes [11, 23, 30, 38], Extended solitons and soliton-chains [40], oscillatory-like [39] eigenmodes
11	Interpretational scheme	By graphical and numerical analyses	Numerical analyses not done [11, 23, 30, 38]
12	Exact mode-patterns	Both electrostatic and self-gravitational fluctuations are studied by analytical tests, followed by numerical analyses	Electrostatic and self-gravitational fluctuations are not studied by numerical analyses [11, 23, 30, 38]

13	Nature of eigenmodes	Low-frequency gravito-electrostatic eigenmodes on the *Jeansian* scales	Dust-acoustic eigenmodes [11, 30, 39], Ion-acoustic eigenmode [23, 38]
14	Deviation from quasi-neutrality (electrostatic) and mass-neutrality (gravitational)	Very small for weakly nonlinear perturbation	Not analyzed [11, 23, 30, 38-40]
15	Geometrical dynamics of the plasma species	Phase trajectories of both the Columbic and Newtonian particles are well studied	Not studied [11, 23, 30, 38-40]
16	Ratio of eigenmode amplitudes	$\Phi_1/\Psi_1 \approx 3.8$, for weakly nonlinear modes; and $\Phi/\Psi \approx 2.5$, for fully nonlinear modes (both in normalized form)	Not shown [11, 23, 30, 38-40]
17	Spatiotemporal (3-D) eigenmode patterns to confirm temporal stability	Shown for both electrostatic and self-gravitational fluctuations	Not shown [11, 23, 30, 38-40]
18	Effect on amplitude for increasing m_d, n_{io}, n_{eo}, n_{do} and Z_d	Shown for both the electrostatic and self-gravitational fluctuations (in both weakly and strongly nonlinear cases)	Not shown for any of the cases [11, 23, 30, 38-40]
19	Effect of dust-charge fluctuations	Soliton-like nonlinear eigenmodes exist without dust-charge fluctuations	Solitary eigenmodes exist if dust-charge fluctuation is neglected from the KdV equation derived originally with dust-charge fluctuations [23]

20	Contribution of the ion-inertia	Specifically shown in both the weakly and strongly nonlinear fluctuations (in minor quantitative enhancement only)	Not shown [11, 23, 30, 38-40]
21	Energy-integral equations (Sagdeev pseudo-potential approach)	Derived for both the electrostatic and self-gravitational cases with effective ion-inertia	Yet to be studied for self-gravitational case [20, 41]
22	Strongly nonlinear eigenmodes	Solitary eigenmodes	Shock-like eigenmodes [41]
23	Ratio of the electro-gravitational Sagdeev potentials	$V_E(\Phi,\Psi)/V_G(\Phi,\Psi)$ $\approx 2\times10^{1}$	Not shown [41]

8.5 CONCLUSIONS

In conclusion, we propose an atypical hydrodynamic model to study the properties of both the weakly and strongly nonlinear wave dynamics of gravito-electrostatically coupled collisional, unmagnetized dusty plasma of infinite extension. It treats the gravitating massive dust grains with negligible partial ionization and the gravitating ions as inertial fluids, but the thermal electrons as the inertialess Boltzmann-distributed species amid all the significant collisional effects retained on the astrophysical hydrodynamic scales of space and time.

The main aim is successfully focused upon investigating the influence of self-consistent dynamic ion-inertial effects on the stability behavior of the grainy cloud, in both the regimes of perturbation, weak and strong. Procedural application of standard multiple scaling techniques reduces the basic plasma structure equations into a unique pair of the decoupled Korteweg-de Vries (KdV) system, with no source or sink due to the static dust-charge considered, governing the weakly nonlinear gravito-electrostatic fluctuations. In contrast, the fully nonlinear counterparts are strategically shown to dynamically evolve as a new gravito-electrostatically coupled pair of the Sagdeev energy-integral equations. Numerical shape-analyses predict the excitation of two distinct

eigenmode classes, electrostatic compressive solitons and self-gravitational rarefactive solitons, with singular parametric features in the framework of interstellar wide-range parameter regimes portrayed in detail. A detailed comparison on the consistency of our results in the light of previous works is presented. The main possible conclusive remarks, are briefly highlighted as follows.

(1) We study the weakly and strongly nonlinear classes of gravito-electrostatic fluctuation modes in unmagnetized, collisional, self-gravitating DMC for the first time with the active ion-inertial correction taken into account on the relevant scales of space and time.

(2) The weakly nonlinear gravito-electrostatic fluctuations are governed by a pair of gravito-electrostatically decoupled KdV equations (equations (8.8), (8.11)) obtained by multiscale analysis within the framework of the point-charge (Coulombic) and point-mass (Newtonian) approximations.

(3) In contrast with the above, the strongly nonlinear gravito-electrostatic fluctuations are ruled by a unique pair of gravito-electrostatically coupled energy-integral equations (equations (8.22), (8.29)) obtained by the Sagdeev pseudo-potential approach under well justified set of sensible boundary conditions.

(4) In both the formalisms, the electrostatic and self-gravitational potential fluctuations co-evolve as compressive $(\Phi > 0)$ and rarefactive $(\Psi < 0)$ solitary eigenmode spectral-patterns (Figures 8.2-8.7) in dynamical response to the background collective plasma wave oscillations, respectively. Their scale-invariant structural signatures are found to be in good correspondence with the experimentally detected solitary waves in collision-dominated plasmas [12-13]. The multi-space satellite-based observations, like Freja, Viking, FAST, etc., [1, 16-19] and earlier theoretical investigations by others [1,11, 24, 30, 32, 36] as well do support our findings.

(5) The gravito-electrostatic eigenmode-amplitude is noticed to possess a direct sensitive correlation with different plasma parameters of interstellar worth. It is interesting to note that the equilibrium density of the inertial ions play a destabilizing influential role leading to enhanced self-gravitational effects by reorganizing the fluctuation amplitudes towards establishing a new gravito-electrostatic equilibrium setup (e. g., Figures 8.2, 8.4, 8.7). This implies that the considered ion-inertial dynamics, even if the neutral dust dynamics is totally ignored for idealization of calculation, can significantly modify the dynamics of nonlinear wave propagations of gravito-electrostatic origin in an extended dusty cloud.

(6) The existential criterion for the gravito-electrostatic solitary eigenmodes, as investigated in our non-fluctuating dust-charge model, goes well with the earlier predictions on the gravitating dust-affected solitary wave reality [23].

(7) In parametric sense, plasma-parameter windows for the existence of the solitary structures for a wide-range of the grain-mass distribution ($10^{-13} < m_d < 10^{-10}$ kg), the equilibrium dust-population density ($10^{-1} < n_{do} < 10^{3}\,\mathrm{m}^{-3}$) and the equilibrium gravitating ion-population density ($10^{4} < n_{io} < 10^{6}\,\mathrm{m}^{-3}$) are explored [37].

(8) The analytical, numerical and graphical analyses show and confirm that, in the adopted interstellar parameter space, the electrostatic fluctuations dominate over the self-gravitational counterparts. Accordingly, for developing an exact gravito-electrostatically balanced structure, the grain-mass should be so small as to make its charge-to-mass ratio remain large. This, in turn, causes the Coulombic and the Newtonian forces get comparable leading to equilibrium structure, which goes quite well with the previous reports by others [1, 11, 30].

(9) The phase portraits of both the Coulombic and Newtonian dynamics reveal a conservative nature of the fluctuations, as the trajectories throughout evolve as closed-form structures. For different plasma parameter-variations, the geometrical trajectories overlap over one another at the potential value corresponding to that near the cloud center. Therefore, it is pertinent to add that the central constituent of the cloud surrounds the most stable fixed point. The phase trajectories start to get slightly separated (alienated) from one another as the potential increases (decreases) in magnitude from the center outwards. This reveals that the cloud gets gradually more unstable at spatial points away from the cloud center.

(10) Lastly, the fluctuation spectral patterns, as presented here, exist in a number of explored clouds, which have been testified by various spacecraft instrumentations, on-board multi-space satellite reports and experimental findings [3; and references therein). Important examples of dusty clouds supporting such wave spectra are *Lynds 204 Complex*, *Barnard 68*, and so forth.

We must finally admit that ignoring the neutral fluid dynamics, frictionally coupled with the collapsing plasma cloud via gravitational force field, is not so physically realistic in understanding the formation processes of stars and other bounded *Jeansian* structures. That is why, in both the formalisms of weak-strong nonlinearities as presented here, the electrostatic fluctuation strength exceeds the self-gravitational complements in strength ($\Phi_1/\Psi_1 \approx 3.8$, $\Phi/\Psi \approx 2.5$), as already

discussed before. However, in spite of such simplifications and limitations, our model analyses could be used to demonstrate a clear theoretical picture about the gravito-electrostatic fluctuation spectral patterns prevailing in rarer interstellar cloudy media, where, the effects of excluded neutral particle dynamics may be insignificant. In consequence, further necessary refinements are to be incorporated in our explorative analyses, which are left out now for new themes of future studies.

REFERENCES

1. Verheest, F. *Waves in Dusty Space Plasmas*, Kluwer Academic Publishers, Dordrecht, Netherlands, 2000.
2. Spitzer, L., Jr. *Physical Processes in the Interstellar Medium*, WILEY-VCH Verlag GmbH & Co. KGaA, Weinheim, 2004.
3. Watkins, R., et al. Nonlinear waves and solitons in molecular Clouds, in The Physics and Chemistry of Interstellar Molecular Clouds, Proceedings of the 2nd Cologne–Zermatt Symposium Held at Zermatt. Switzerland, 21–24 September 1993, G. Winnewisser, & G. C. Pelz, eds., Springer, New York, 1995, 115-117.
4. Infled, E. & Rowlands, G. *Nonlinear Waves, Solitons and Chaos*, 2nd ed., Cambridge University Press, New York, 2000.
5. Shukla, P. K. & Mamun, A. A. *Introduction to Dusty Plasma Physics*, IOP, Bristol and Philadelphia, 2002.
6. Chen, J.-H. and Wei, N.-X. Effects of adiabatic dust charge fluctuation and particles collisions on dust-acoustic solitary waves in three-dimensional magnetized dusty plasmas, *Commun. Theor. Phys.* **51**, 524-528, 2009.
7. Gupta, M. R., et al. Effect of nonadiabaticity of dust charge variation on dust acoustic waves: Generation of dust acoustic shock waves, *Phys. Rev. E* **63**, 046406(1)-046406(9), 2001.
8. Xiao, De-L., et al. Evolution of nonlinear dust-ion-acoustic waves in an inhomogeneous plasma, *Phys. Plasmas* **13**, 052308(1)-052308(7), 2006.
9. Misra, A. P., et al. Acoustic waves in a self-gravitating collisional dusty plasma, *Phys. Scr.* **71**, 207-2012, 2005.
10. Asaduzzaman, M. and Mamun, A. A. Compressive and rarefactive dust-acoustic gardner solitons beyond the K-dV limit with two-temperature ions dusty plasma, *Astrophys. Space Sci.* **341**, 535-542, 2012.

11. Burman, S. and Chowdhury, A. R. Solitary waves in self-gravitating dusty plasma, *Chaos Sol. Fract*. **13**, 973-979, 2002.
12. Barkan, A., et al. Laboratory observation of the dust-acoustic wave mode, *Phys. Plasmas* **2**, 3563-3565, 1995.
13. El-Zein, Y., et al. Excitation of ion acoustic solitons from grids, *J. Plasma Phys.* **61**, 161-168, 1999.
14. Dwivedi, C.B., et al. Pulsational mode of gravitational collapse and its impact on the star formation, *Astron. Astrophys*. **345**, 1049-1053, 1999.
15. Pandey, B. P., et al. The Pulsational mode in the presence of dust charge fluctuations, *Phys. Scr.* **65**, 513-517, 2002.
16. Ergun, R. E., et al. FAST satellite observation of large-amplitude solitary structure, *Geophys. Res. Lett.* **25**, 2041-2044, 1998.
17. Franz, J. R. and Kintner, P. M. POLAR observations of coherent electric field structures, *Geophys. Res. Letts*. **25**, 1277-1280, 1998.
18. Berthomier, M., et al. Scaling of 3D solitary waves observed by FAST and POLAR, *Geophys. Res. Letts.* **30**, 1-5, 2003.
19. Omur, Y., et al. Electrostatic solitary waves carried by diffused electron beams observed by the Geotail spacecraft, *J. Geophys. Res.* **104**, 14627-14637, 1999.
20. Mace, R. L. and Hellberg, M. A. Dust-acoustic double layers: ion inertial effects, *Planet. Space Sci.* **41**, 235-244, 1993.
21. Pandey, B. P. and Dwivedi, C. B. Ion dynamics and gravitational instability of a dusty plasma, *J. Plasma Phys.* **55**, 395-400, 1996.
22. Merlino, R. L. and D'Angelo, N. Electron and ion inertia effects on current-driven collisional dust acoustic, dust ion acoustic, and ion acoustic instabilities, *Phys. Plasmas* **12**, 054504(1)--054504(4), 2005.
23. Paul, S. N., et al. On the existence of ion-acoustic solitary waves in a gravitating dusty plasma having charge fluctuation, *Czech. J. Phys.* ***54***, 1453-1460, 2006.
24. Ghosh, S., et al. Effect of finite ion inertia and dust drift on small amplitude dust acoustic soliton, *Planet. Space Sci.* **48**, 609-614, 2000.
25. Alinejad, H. Dust ion-acoustic solitary and shock waves in a dusty plasma with non-thermal electrons, *Astrophys. Space Sci*. **327**, 131-137, 2010.

26. Washimi, H. and Taniuti, T. Propagation of ion-acoustic solitary waves of small amplitude, *Phys. Rev. Letts.* **17**, 996-998, 1966.
27. Sagdeev, R. Z. Cooperative phenomena and shock waves in collisional plasmas, in *Reviews of Plasma Physics*, M. A. Leontovich, ed., Consultants Bureau, New York, 1966, 23-91.
28. Cadez, V. M. Applicability problem of Jeans criterion to a stationary self-gravitating cloud, *Astron. Astrophys.* **235**, 242-244, 1990.
29. Vranjes, J. Gravitational instability problem of nonuniform medium, *Astrophys. Space Sci.* **213**, 139-142, 1994.
30. Verheest, F. and Shukla, P. K. Nonlinear waves in multispecies self-gravitating dusty plasmas, *Phys. Scr.* **55**, 83-85, 1997.
31. Jacobs, C. and Poedts, S. A polytropic model for the solar wind, *Adv. Space. Res.* **48**, 1958-1966, 2011.
32. Maharaj, S. K., et al. Existence domains of slow and fast ion-acoustic solitons in two-ion space plasmas, *Phys. Plasmas* **22**, 032313(1)-032313(11), 2015.
33. Leblond, H. The reductive perturbation method and some of its applications, *J. Phys. B: At. Mol. Opt. Phys.* **41**, 043001(1)-043001(35), 2008.
34. Vranjes, J. and Tanakaa, M. Y. On gravity induced electric field in space plasmas, *Phys. Scr*. **71**, 325-328, 2005.
35. Shukla, P. K. and Mamun, A. A. Solitons, shocks and vortices in dusty plasmas, *New J. Phys.* **5**, 17.1-17.37, 2003.
36. Shukla, P. K. Dust Plasma Interaction in Space, Nova Science Publishers, New York, 2002.
37. Borah, B., et al. Atypical gravito-electrostatic fluctuations in presence of active ion-inertial dynamics, *Journal of Plasma Physics*, 2015 (under minor review).
38. Paul, S. N., et al. Ion-acoustic solitary waves in a self-gravitating dusty plasma having two-temperature electrons, *World Academy of Sci., Eng. and Tech.* **5**, 472-477, 2011.
39. Guo, Z.-R., et al. Nonlinear acoustic waves in a collisional self-gravitating dusty plasma, *Chin. Phys. B.* **19**, 115203(1)-115203(5), 2010.
40. Karmakar, P. K. Nonlinear stability of pulsational mode of gravitational collapse in self-gravitating hydrostatically bounded dust molecular cloud, *Pramana- J. Phys.* **76**, 945-956, 2011.
41. Misra, A. P. and Chowdhury, A. R. Dust-acoustic waves in a self-gravitating complex plasma with trapped electrons and nonisothermal ions, *Eur. Phys. J. D* **37**, 105-113, 2006.